Faculty Publications                                  Chemical Engineering, Department of

# Parameter Sensitivity and Optimization Predictions of a Hydrogen/Oxygen Alkaline Fuel Cell Model

Michael C. Kimble
*Texas A & M University - College Station*

Ralph E. White
*University of South Carolina - Columbia*, white@cec.sc.edu

Follow this and additional works at: https://scholarcommons.sc.edu/eche_facpub

Part of the Chemical Engineering Commons

# Parameter Sensitivity and Optimization Predictions of a Hydrogen/Oxygen Alkaline Fuel Cell Model

## Michael C. Kimble*,[1] and Ralph E. White*

*Department of Chemical Engineering, Texas A&M University, College Station, Texas 77843-3122*

## ABSTRACT

A mathematical model is used to predict parameter sensitivities and optimal design parameters for a hydrogen/ oxygen alkaline fuel cell. A sensitivity analysis of the various transport and electrode kinetic parameters indicates which parameters have the most influence on the predicted current density and over which range of potentials these parameters affect the fuel-cell performance the most. This information can be used to decide which parameters should be optimized or determined more accurately through further modeling or experimental studies. The effect of various design parameters on the limiting current density are investigated to determine if optimal values exist for the parameters. The optimal electrode thicknesses for the anode and cathode reaction layers and the gas- and liquid-phase porosity in the cathode reaction layer are determined by maximizing the power density. These parameter sensitivities and optimal design parameters can help in the development of better three-phase electrodes and separators for the alkaline fuel cell.

In designing high-performance alkaline fuel cells, there are various attributes that can significantly influence the system. Such attributes might be the gas- and liquid-phase porosities, reaction layer and separator thicknesses, or the number of gas-liquid sites in the three-phase electrodes. One way to investigate the relative importance of these parameters is to use a mathematical model that describes the chemical, electrochemical, and physical processes occurring in the fuel cell. Typically, models of single, three-phase electrodes are used in determining polarization losses and optimal design parameters (1, 2). However, these models do not consider any interactions between the anode, cathode, and separator which can significantly alter the performance of the system as well as alter the optimal values for certain parameters. A previously developed mathematical model of the alkaline fuel cell (3) is used to analyze the effects of some of the more influential parameters on the predicted current density. A sensitivity analysis is performed on various parameters to determine which parameters are the most influential in increasing or decreasing the current density. This information can indicate the direction one should take in order to design better fuel cells. The results of the sensitivity analysis can also suggest which parameters should be obtained with more accuracy through further modeling studies or through experimentation.

To achieve high performance in the alkaline fuel cell, various design parameters can be optimized so that the fuel cell will deliver the maximum attainable power density. The important design parameters in the alkaline fuel cell are the thicknesses of the anode and cathode diffusion and reaction layers ($L_D$, $L_R$), separator thickness ($L_S$), electrode conductivity ($\sigma$), gas and liquid phase porosities ($\epsilon^g$, $\epsilon^l$), gas-liquid interfacial surface area ($a^g$), and the liquid-solid interfacial surface area ($a^l$). By using the detailed model of the alkaline fuel cell, these parameters are investigated in order to determine if an optimal value exists for each parameter. In order to understand better the effects of the design parameters on the fuel-cell performance, a summary of the phenomenological equations that describe the alkaline fuel cell will be presented next. The sensitivity of the model predictions to various parameters will then be examined, followed by the determination of the optimal design parameters to maximize the alkaline fuel cell's power density.

## Phenomenological Equations

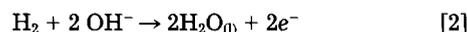The reactions occurring in the alkaline fuel cell are the reduction of oxygen at the cathode

Cathode
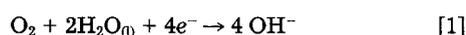
$$O_2 + 2H_2O_{(l)} + 4e^- \rightarrow 4\,OH^- \qquad [1]$$

and the oxidation of hydrogen at the anode

Anode

$$H_2 + 2\,OH^- \rightarrow 2H_2O_{(l)} + 2e^- \qquad [2]$$

so that the overall reaction is the production of water.

Total

$$H_2 + \frac{1}{2}O_2 \rightarrow H_2O_{(l)} \qquad [3]$$
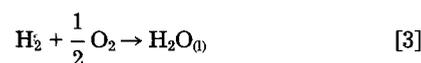
A macrohomogeneous model that predicts the cell performance based on these reactions was developed by Kimble and White (3). Gas-phase diffusional resistances were accounted for by calculating partial pressure drops for the hydrogen, oxygen, and water vapor in the gaseous pores. Liquid-phase diffusional resistances were considered by accounting for the concentration distributions of the dissolved oxygen and hydrogen in the electrolyte. Ohmic resistances were accounted for by calculating the potential drops in the solid and solution phases. Ionic resistances were considered by calculating the concentration distributions of the ionic species. A schematic of the alkaline fuel cell is shown in Fig. 1, which shows the various regions that are considered in the model. The phenomena occurring in the anode and cathode gas-diffusion layers, anode and cathode reaction layers, and the separator region are described by the steady-state form of the equation of continuity in a porous media

$$\nabla \cdot \mathbf{N}_i = R_i^p + R_i^e \qquad (i = O_2, H_2, H_2O, +, -, o) \qquad [4]$$

where the flux, $\mathbf{N}_i$, is expressed by the Stefan-Maxwell equation for gas-phase transport

$$\nabla y_i = \sum_{j=1}^{2} \frac{RT}{P\mathfrak{D}_{i,j}^g}(y_i\mathbf{N}_j - y_j\mathbf{N}_i) \quad (i, j = O_2 \text{ or } H_2, H_2O) \qquad [5]$$

and by the ionic flux expression for solution phase transport

$$\mathbf{N}_i = -\mathfrak{D}_i^l \nabla C_i - z_i u_i FC_i\nabla\phi + C_i v^\blacksquare \quad (i = O_2, H_2, +, -, o) \; [6]$$

Note that Eq. [5] and [6] contain effective diffusivities, $\mathfrak{D}_i$, which are related to the free-stream diffusivities by a porosity and tortuosity factor

$$\mathfrak{D}_i = \frac{\epsilon D_i}{\tau} \qquad [7]$$

The gas-dissolution rate, $R_i^p$, can be approximated by

$$R_i^p = -a^g\mathfrak{D}_i^l\left(\frac{H_iP_i - C_i}{\delta}\right) \qquad [8]$$
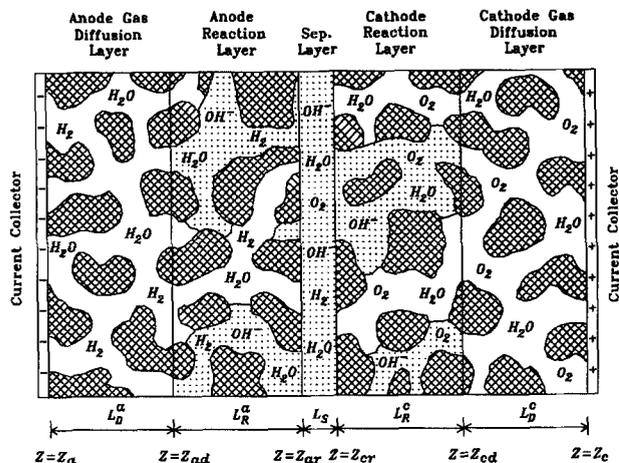
**Fig. 1. Schematic of an alkaline fuel cell.**

where it is assumed that equilibrium is established at the gas-liquid interface. Note that this rate expression follows the thin-film theory for gas dissolution where $\delta$ is the diffusion-layer thickness and $a^g$ is the interfacial surface area between the gas- and liquid-phases in the electrode. The electrochemical reaction rate, $R_i^e$, in Eq. [4] is given by

$$R_i^e = \frac{s_i a^l i}{nF} \qquad [9]$$

where the local current density, $i$, is expressed by the Butler-Volmer electrochemical rate expression

$$i = i^o \left[ \prod_i \left( \frac{C_i}{C_i^r} \right)^{p_i} \exp\left( \frac{\alpha^a nF}{RT} \eta \right) \right.$$
$$\left. - \prod_i \left( \frac{C_i}{C_i^r} \right)^{q_i} \exp\left( \frac{-\alpha^c nF}{RT} \eta \right) \right] \qquad [10]$$

The overpotential, $\eta$, in Eq. [10] is given by

$$\eta = E - \phi - U_{ref} \qquad [11]$$

where the solid potential, $E$, is described by Ohm's law

$$\nabla E = -\frac{I}{\sigma} \qquad [12]$$

Equations [4]-[12] represent the basic phenomenological equations necessary to describe the behavior in the various regions of the alkaline fuel cell. It should be noted that these equations are solved numerically by setting the cell potential, $E_{cell}$, and calculating the cell current density, $I$, or

the power density, $P$ ($=IE_{cell}$). The model parameters associated with these equations are shown in Table I. Other supporting parameter values such as diffusivities and Henry's law constants that are not shown in Table I can be found in the original model development (3).

## Sensitivity Analysis

In order to determine the relative importance of the transport, kinetic, and structural parameters on the fuel cell's performance, a sensitivity analysis can be applied. The sensitivity analysis can indicate which parameters have the largest influence on the predicted current density and, also, over which range of cell potentials the parameters have the most influence. Additionally, the sensitivity analysis can indicate which parameters are capable of being estimated when the model is used in conjunction with experimental data and a parameter estimation technique. That is, if a small perturbation in a parameter does not significantly change the predicted current density, then that parameter could assume a large range of values, all of which will give the same performance. The sensitivity coefficient can be defined as the difference in the base-case current density from the predicted current density for a small dimensionless perturbation in a parameter $j$, while holding all other parameters constant

$$\frac{\partial I}{\partial \ln \theta_j} = \frac{I - I^*}{\dfrac{\theta_j - \theta_j^*}{\theta_j^*}} \, (A/cm^2) \qquad [13]$$

where $\theta_j^*$ and $I^*$ are the base-case parameter value and current density, respectively. Hence, large sensitivity coefficients indicate that the parameter of interest significantly influences the current density. Large sensitivity coefficients may also indicate which parameters should be obtained with more accuracy through further modeling or experimental studies. That is, if the value for a parameter is not accurately known and the parameter has a large sensitivity coefficient, then that parameter value should be ascertained with more accuracy to gain confidence in the model predictions.

All sensitivity coefficients calculated for this work were accomplished by increasing the parameter of interest by 5% over the base-case value (shown in Table I) and calculating the resulting change in the current density from the base-case current density. This was performed over the potential ranges of (0.8-0.85 V), (0.85-0.93 V), and (0.93-1.1 V) representative of the concentration, ohmic, and activation polarization regions, respectively, for the conditions of the fuel-cell simulation. By investigating the sensitivity coefficients in these three potential regions, the effects of the parameters on the current density can be investigated under conditions of the various forms of polarization where the fuel cell may actually operate. It should be

**Table I. Base-case parameter values for the alkaline-fuel-cell simulation.**

| | |
|---|---|
| Structural parameters: | |
| Anode and cathode diffusion-layer thicknesses ($L_D^a$, $L_D^c$) | 0.025 cm |
| Anode and cathode reaction-layer thicknesses ($L_R^a$, $L_R^c$) | 0.005 cm |
| Separator thickness ($L_S$) | 0.005 cm |
| Porosities: | |
| Anode and cathode diffusion-layer gas-phase porosities ($\epsilon_{D,a}^g$, $\epsilon_{D,c}^g$) | 0.70 |
| Anode and cathode reaction-layer gas-phase porosities ($\epsilon_{R,a}^g$, $\epsilon_{R,c}^g$) | 0.05 |
| Anode and cathode reaction-layer liquid-phase porosities ($\epsilon_{R,a}^l$, $\epsilon_{R,c}^l$) | 0.65 |
| Separator porosity ($\epsilon_S$) | 0.80 |
| Electrode kinetic parameters: | |
| Anodic and cathodic exchange transfer currents ($i_a^o \cdot a_a^l$, $i_c^o \cdot a_c^l$) | 0.60 A/cm³ |
| Anodic and cathodic diffusional film areas ($a_a^g/\delta_a$, $a_c^g/\delta_c$) | $5 \times 10^8$ cm⁻² |
| Anodic transfer coefficient for hydrogen oxidation ($\alpha_{H_2}^a n_a$) | 1.5 |
| Cathodic transfer coefficient for oxygen reduction ($\alpha_{O_2}^c n_c$) | 1.5 |
| Anode and cathode electrode conductivities ($\sigma^a$, $\sigma^c$) | 5.0 S/cm |
| Hydrogen gas reaction order ($p_{H_2}$) | 1.0 |
| Oxygen gas reaction order ($q_{O_2}$) | 0.5 |
| Operating conditions: | |
| Initial electrolyte concentration ($C_e$) | 7 N |
| Temperature ($T$) | 80°C |
| Anode and cathode inlet pressures ($P^a$, $P^c$) | 4.1 atm |
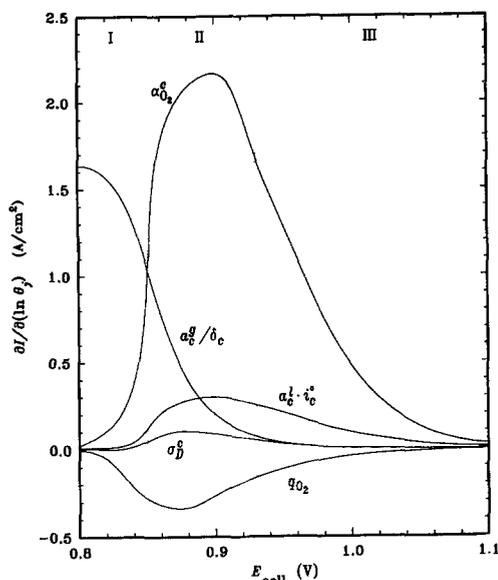
**Fig. 2. Sensitivity of the model predictions to cathode parameters for the concentration (I), ohmic (II), and activation (III) polarization regions.**

noted that since these three forms of polarization do not act independently of one another, it should not be concluded that the predicted current densities are a result of a single form of polarization. The sensitivity coefficients for various parameters are shown in Fig. 2 and 3 for parameters specific to the cathode and anode, respectively. As shown in the activation and ohmic regions, the model predictions are most sensitive to the transfer coefficients, liquid-phase specific surface area, and the reactant-gas reaction orders. Since the model predictions are extremely sensitive to the transfer coefficients as governed by the exponential terms in the Butler-Volmer expression, Eq. [10], small perturbations in the transfer coefficients can significantly affect the predicted current density. Unfortunately, obtaining accurate values for the transfer coefficients is difficult since they vary too much depending on the temperature, cell potential, and electrocatalyst. Parameter estimation techniques could be used to fit the model to reliable experimental data by predicting the values for the transfer coefficients. This may necessitate a reformulation of the Butler-Volmer expression as shown by Evans and White (4) to avoid numerical difficulties in the parameter estimation method.
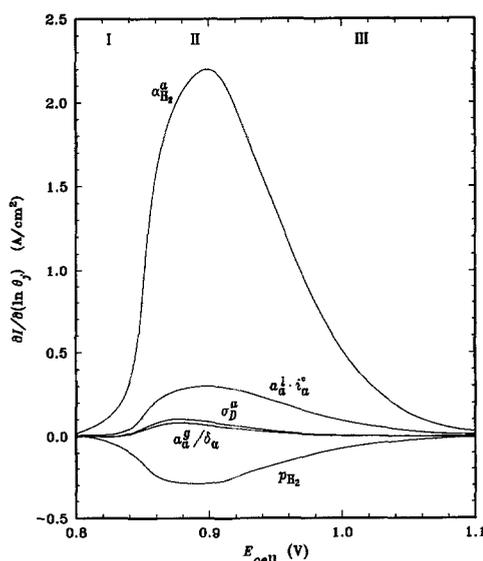
The model predictions show little sensitivity to small perturbations in the conductivities of the cathode and anode diffusion regions as shown in Fig. 2 and 3, respectively. The dependence of the model predictions on the conductivities in the reaction layers was even less pronounced than in the diffusion layers. The relative insensitivity of the model predictions to the ratio of $a_a^g/\delta_a$ over the entire range of cell potentials indicates that the dissolution of hydrogen gas into the electrolyte is not rate limiting. The most influential parameter in the concentration polarization region is $a_c^g/\delta_c$ which governs how much oxygen gas dissolves into the electrolyte through Eq. [8]. Note that the liquid-phase diffusivity and the concentration difference, $H_{O_2}P_{O_2} - C_{O_2}$, govern how fast oxygen dissolves into the electrolyte. Clearly, increasing the solubility of oxygen in KOH or increasing the diffusivity of oxygen in the electrolyte will increase the rate of oxygen dissolution.

The effects of fuel cell thickness on the predicted performance are shown in Fig. 4 where the model predictions are most sensitive to the cathode reaction-layer thickness followed by the anode reaction-layer and separator thickness. The anode and cathode gas-diffusion-layer thicknesses are shown to have little effect on the model predictions. It is also apparent in Fig. 4 that the limiting current density can be increased by increasing the cathode reaction-layer thickness or by decreasing the separator thickness. However, as will be shown later, increasing the cathode reaction-layer thickness too much can degrade the performance.

The effects of porosity on the model predictions are shown in Fig. 5, where $\epsilon_{R,c}^l$ has the largest influence on the model predictions followed by $\epsilon_{R,c}^g$, $\epsilon_S$, and $\epsilon_{R,a}^l$. Increasing the gas-phase porosities in the diffusion layers and in the anode reaction layer showed no change in the model predictions.

## Current Density Optimization

The previous analysis on the sensitivity coefficients showed that small perturbations in design parameters could yield significant improvements in the current density. However, the sensitivity analysis does not allow a quantitative prediction on what values the design parameters should have in order to provide the best performance. By using the mathematical model of the alkaline fuel cell, various design parameters can be optimized so that the system achieves the maximum attainable power density. From Fig. 4, it can be seen that the anode and cathode reaction-layer thicknesses and the separator thickness have the most effect on the performance. Calculating the limit-



**Fig. 3. Sensitivity of the model predictions to anode parameters for the concentration (I), ohmic (II), and activation (III) polarization regions.**
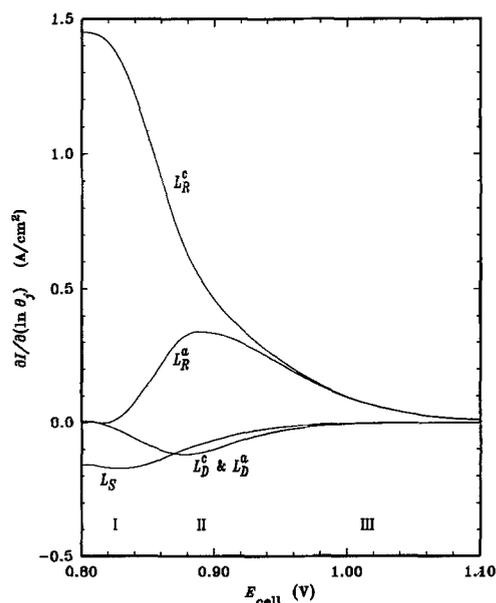


**Fig. 4. Sensitivity of the model predictions to changes in fuel-cell thickness for the concentration (I), ohmic (II), and activation (III) polarization regions.**
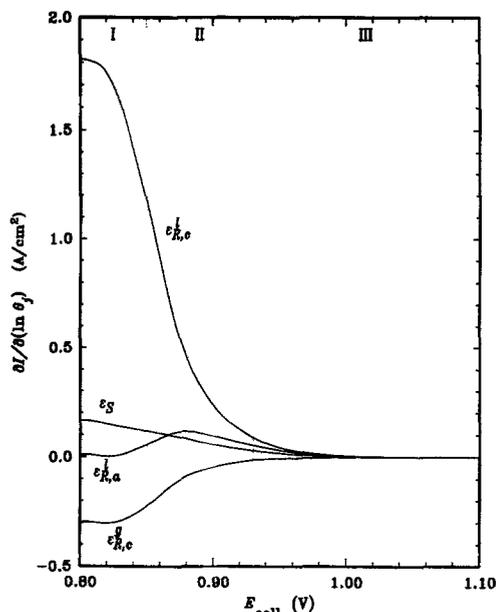
Fig. 5. Sensitivity of the model predictions to changes in porosity for the concentration (I), ohmic (II), and activation (III) polarization regions.



Fig. 7. Sensitivity of the model predictions to changes in diffusivity and solubility for the concentration (I), ohmic (II), and activation (III) polarization regions.

ing current density for these parameters as they are varied individually over a 20 to 300 μm range with the others set equal to their base-case values (Table I) gives the results shown in Fig. 6. As shown in Fig. 6, a maximum occurs in the limiting current density for $L_R^a$ at about 40 μm and for $L_R^c$ at about 225 μm. The separator thickness does not show a maximum in the limiting current density indicating that its thickness should be as small as possible. Kenjo and Kawatsu (5) measured a flat limiting-current density of about 1.5 A/cm² corresponding to a reaction layer thickness of 100 to 270 μm for an oxygen electrode. Although different operating conditions were used, the location of the optimal thickness range in Fig. 6 for $L_R^c$ is similar to that obtained by Kenjo and Kawatsu (5). It has commonly been thought that increasing the reaction-layer thickness should increase the limiting current density since more reaction sites are present in the electrode. However, according to our model, the reason for the decrease in the limiting current density beyond an optimal thickness is due to a lowering of the oxygen gas solubility and liquid-phase diffu-
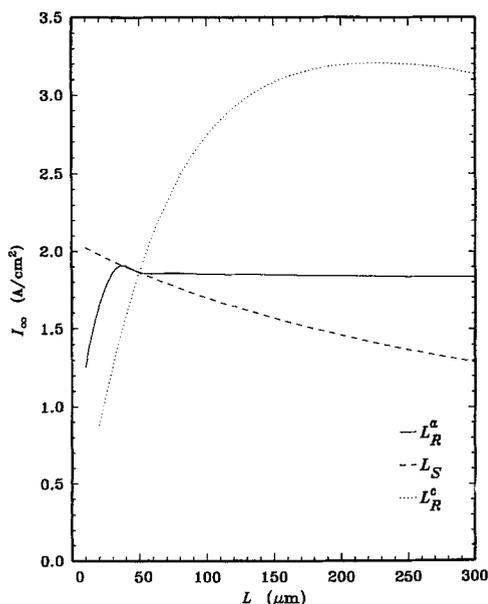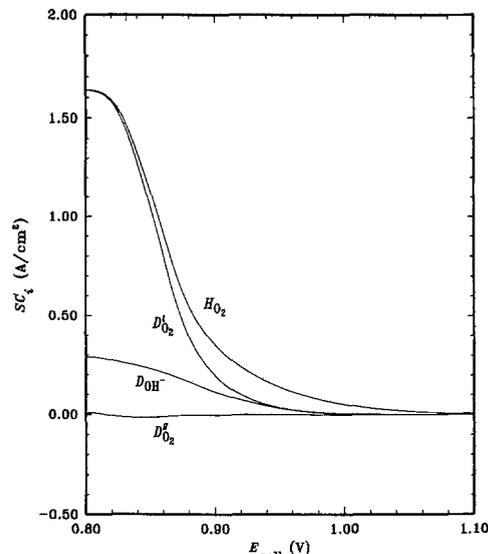
sivity, not to gas-phase diffusional resistances as suggested by Kenjo and Kawatsu (5) and by Bjornbom (6). When the cathode reaction layer is increased, more hydroxide ions are produced in the cathode as given by the oxygen reduction reaction, Eq. [1]. According to experimental observations, this increase in the KOH concentration decreases the solubility of oxygen in KOH (7, 8) and decreases the diffusivity of dissolved oxygen in KOH (8, 9). A sensitivity analysis of these parameters is shown in Fig. 7 along with the sensitivity of the oxygen gas-phase diffusivity and the ionic diffusivity. Clearly, the sensitivity of the model predictions to the oxygen gas-phase diffusivity, $D_{O_2}^g$, and the ionic diffusivity, $D_{OH^-}$, is insignificant in comparison to the oxygen solubility (given in the form of a Henry's law constant, $H_{O_2}$) and the liquid-phase diffusivity, $D_{O_2}^l$. Hence, the performance of the fuel cell can be improved by increasing the cathode reaction-layer thickness up to a certain critical thickness which upon further increasing the thickness causes a performance degradation due to a lower gas solubility and a lower liquid-phase diffusivity.

The sensitivity analysis for the porosity parameters, Fig. 5, show that the concentration and ohmic polarization regions are significantly influenced by the various porosities. To investigate the optimal values for these porosities, the limiting current density was calculated for different parameter settings for the liquid-phase porosities. These results are shown in Fig. 8. Note that the anode and cathode reaction layers were assumed to have a total porosity of 0.7, causing a constraint for the gas and liquid phase porosities

$$0.7 = \epsilon_R^g + \epsilon_R^l \qquad [14]$$

As shown in Fig. 8, increasing $\epsilon_{R,a}^l$ does not cause any noticeable difference in the predicted limiting-current density. However, in the cathode a dramatic increase in the limiting current density occurs up to an optimal porosity of about 0.695, where a rapid decline in the limiting current density occurs upon further increasing the porosity. Since the model treats the gas-phase transport as occurring by molecular diffusion and convection, only a small fraction of the total electrode porosity is needed for the gas phase. As the gas-phase porosity approaches a small value (e.g., 0.005), the effective gas-phase diffusivity becomes even smaller through Eq. [7] resulting in mass-transfer limitations for the gas-phase transport. Increasing the separator porosity increases the limiting current density more rapidly at lower porosities than at higher porosities. Since the separator porosity was assumed to be 0.8, further increasing the porosity will result in a slight increase of 30 mA/cm² at the limiting current density. Unfortunately, a
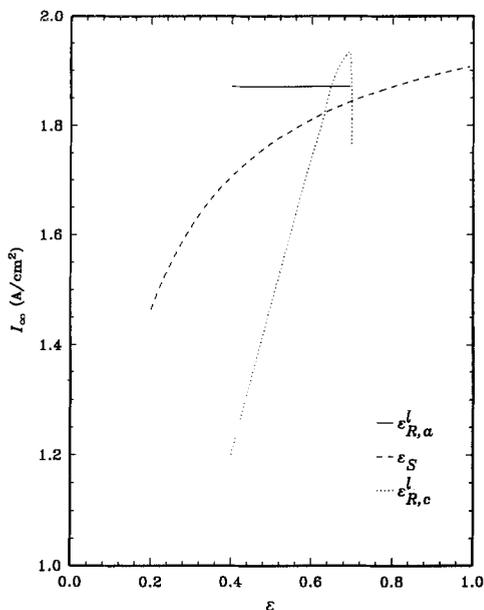


Fig. 6. Effects of the separator and reaction-layer thicknesses on the limiting current density.

**Fig. 8.** Effects of liquid-phase porosity on the limiting current density.



**Fig. 9.** Effects of the gas-liquid and liquid-solid interfacial surface areas.

maximum does not occur in the limiting current density for the separator porosity, preventing an optimal porosity from being recognized. Note that other criteria could be considered in determining an optimal separator porosity in addition to an extremum in the current density such as the separator bubble pressure, mechanical strength of the separator, or lifetime, but this is beyond the scope of this work.

The sensitivity analysis showed that the quantities $a^l \cdot i^o$ and $a^g/\delta$ have an effect on the fuel-cell performance since they affect the liquid-solid electrochemical reaction, $R_i^e$, and the liquid-gas dissolution reaction, $R_i^p$. It should be noted that the product of $a^l$ and $i^o$ always occur together in the model equations as well as the ratio of $a^g$ to $\delta$. This is unfortunate since it prevents the interfacial surface areas, exchange current densities, and the diffusion layer thicknesses from being individually identified. Hence, the parameter combinations, $a^l \cdot i^o$ and $a^g/\delta$, were varied and the current density was calculated by the model as shown in Fig. 9. Note that the performance curve for the parameter combination $a_a^l \cdot i_a^o$ is similar to that obtained for $a_c^l \cdot i_c^o$ and, thus, is not shown in Fig. 9. It should also be noted that $a_a^l \cdot i_a^o$ and $a_c^l \cdot i_c^o$ affect only the kinetics of the electrochemical reactions and not the limiting current density as shown earlier [(3) Fig. 7]. For this reason, calculating the limiting current density for changes in $a^l \cdot i^o$ is meaningless since this parameter combination does not influence the limiting current density as does the $a^g/\delta$ parameter combination. To determine the effects of $a^l \cdot i^o$ on the fuel-cell performance, the current density was predicted in the kinetically controlled region at 0.9 V for $a_c^l \cdot i_c^o$ ranging from about 0.0 to 0.50 A/cm³ as shown in Fig. 9. The predicted current density at 0.9 V shows a sharp increase for $a_c^l \cdot i_c^o$ in the range of 0.0 to 0.1 A/cm³ followed by a gradual increase in the current density as $a_c^l \cdot i_c^o$ is further increased. This result suggests that increases in $a_c^l \cdot i_c^o$ over a certain critical value, approximately 0.4 A/cm³ in Fig. 9, will contribute only a marginal improvement to the current density, indicating that some other phenomena may be limiting the performance of the system.

The limiting current density at 0.75 V was predicted by the model for the anode and cathode parameter combinations, $a^g/\delta$, over the range of 0.0 to 5.0 × 10⁹ cm⁻² as shown in Fig. 9. Increasing $a_a^g/\delta_a$ beyond 2.0 × 10⁸ cm⁻² does not improve the current density at all. Although increasing this parameter combination increases the dissolution rate, $R_{H_2}^p$, of hydrogen gas into the electrolyte as governed by Eq. [8], the dissolution rate for oxygen is still limiting the current density. This is verified by the performance curve for $a_c^g/\delta_c$, where increasing this parameter combination
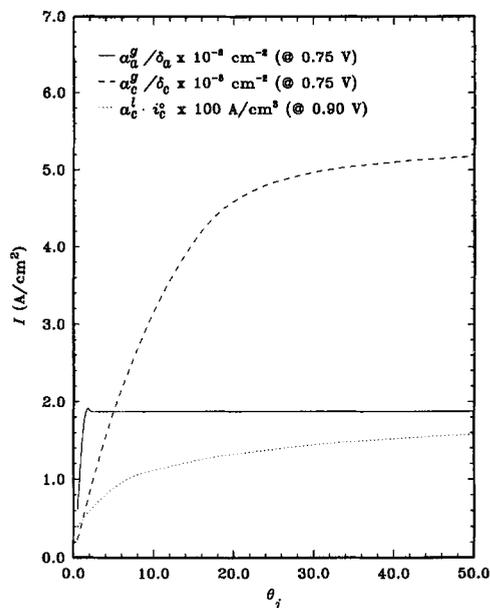
causes an increase in the current density. Since the diffusion-layer thickness, $\delta$, may be difficult, if not impossible, to control, increasing $a_c^g/\delta_c$ by designing three-phase electrodes with large interfacial gas-liquid surface areas will allow more gas to dissolve into the electrolyte to react.

To achieve optimal performance in the fuel cell, the more influential parameters of the model can be used to maximize the predicted current density or power density. It should be noted that other criteria than a maximum current density could be used in formulating an objective function. For example, Newman (10) optimizes an acid fuel cell by considering the average current density and the utilization of hydrogen based on capital, power, and fuel costs. Since the main objectives of this work are to increase the maximum attainable power density, economic factors are not considered. To maximize the power density, an objective function can be defined as

$$\max P(\theta) = E_{cell} \cdot I(\theta, E_{cell}) \qquad [15]$$

where $\theta$ represents a vector of unknown parameters $\theta_j$ and $E_{cell}$ is itself an unknown cell potential. Since the model calculates the total cell current density for a given cell potential, the cell potential is included in the objective function so that it may be optimized along with the unknown design parameters $\theta$. The optimal design parameters and cell potential can be selected such that the power density as given by Eq. [15] is at a maximum.

The results of the sensitivity analysis shown in Fig. 2 to 5 and the single parameter optimal studies shown in Fig. 6 to 9 indicate which parameters can be optimized in Eq. [15]. The anode and cathode reaction layer thicknesses and the liquid-phase porosity in the cathode reaction layer are the only parameters that caused an extremum in the predicted current density. All other parameters investigated here monotonically increased the current density as the parameters were lowered (e.g., $L_S$) or increased (e.g., $a^g$, $a^l$, $\epsilon_S$). Note that the transfer coefficients could be included in the optimization procedure since they have a strong effect on the current density as shown in Fig. 2 and 3. Additionally, the reactant-gas reaction orders, $q_{O_2}$, and $p_{H_2}$ could also be included in the optimization procedure. However, since the transfer coefficients and reaction orders are dependent upon the operating conditions rather than on structural conditions such as thickness and porosity, the transfer coefficients and reaction orders were not considered in the optimization procedure.

The IMSL routine BCONF (11) was used to maximize Eq. [15] by using a quasi-Newton method to determine $L_R^a$, $L_R^c$, $\epsilon_{R,c}^l$, and $E_{cell}$. The optimized values are shown in

**Table II. Optimal parameter values for maximizing the power density.**

| Starting values | Optimized values |
|---|---|
| $L_R^a = 0.005$ cm | $L_R^a = 0.01627$ cm |
| $L_R^c = 0.005$ cm | $L_R^c = 0.02234$ cm |
| $\epsilon_{R,c}^l = 0.65$ | $\epsilon_{R,c}^l = 0.674$ |
| $E_{cell} = 0.75$ V | $E_{cell} = 0.803$ V |

Table II along with their starting values. The optimal cathode reaction-layer thickness in Table II corresponds to about the same optimal value as shown in Fig. 6, whereas a large difference results for the optimal anode reaction-layer thickness. Since increasing $L_R^a$ above 55 μm did not improve the current density as shown in Fig. 6, $L_R^a$ was scaled over a thickness range of 50 to 300 μm using the optimal values in Table II for $L_R^c$, $\epsilon_{R,c}^l$, $E_{cell}$ to investigate whether $L_R^a$ is indeed at an optimal value. The resulting performance curve verified that the optimal anode reaction-layer thickness shown in Table II does cause an extremum in the power density. Using the optimal parameter values other then $E_{cell}$, the performance of the fuel cell was predicted by the model over the potential range of 0.7 to 1.1 V as shown in Fig. 10 in comparison to the base-case performance. As can be seen, a significant improvement in the maximum attainable power density has been achieved just by optimizing the cell potential and three design parameters.

## Summary

A sensitivity analysis of an alkaline fuel-cell model indicates that many parameters can significantly influence the performance of the system, especially in the ohmic and concentration polarization regions. In particular, parameters specific to the oxygen electrode such as the reaction-layer thickness, liquid-phase porosity, gas-liquid interfacial surface area, and the cathodic transfer coefficient have been found to influence significantly the performance. The effect of various design parameters on the limiting current density have been investigated to determine if optimal values exist for the parameters. The model has shown that the anode and cathode reaction layer thicknesses, the liquid-phase porosity in the cathode reaction region, and the cell potential can be optimized to give the maximum attainable power density. The optimal reaction-layer thicknesses are shown to be a compromise among the number of reaction sites, the solubility of the reactant gases, and the liquid-phase diffusivity of the dissolved reactant gases. A small fraction of the total porosity in the cathode reaction region is needed in the gas phase to sustain a high gas-phase diffusion rate while maintaining a large diffusion rate in the liquid phase. The model predictions indicate that the largest improvement in the fuel cell performance will be recognized by increasing the gas-liquid interfacial surface area in the cathode followed by increasing the electrocatalytic activity or liquid-solid interfacial surface area and decreasing the separator thickness from the base-case conditions.

## Acknowledgments

## LIST OF SYMBOLS

| | |
|---|---|
| $a^g$ | interfacial surface area between gas and liquid phases, cm²/cm³ |
| $a^l$ | interfacial surface area between liquid and solid phases, cm²/cm³ |
| $C_i$ | concentration of species $i$, mol/cm³ |
| $D_i$ | free stream diffusivity of species $i$, cm²/s |
| $\mathcal{D}_i$ | effective diffusivity of species $i$, cm²/s |
| $E$ | electrode potential, V |
| $F$ | Faraday's constant, 96,487 C/mol |
| $H_i$ | Henry's constant for species $i$, mol/(cm³-atm) |
| $I$ | total cell current density, A/cm² |
| $I_\infty$ | limiting current density, A/cm² |
| $i$ | local current density, A/cm² |
| $i^o$ | exchange current density, A/cm² |
| $L$ | thickness, cm |
| $n$ | number of electrons transferred |
| $N_i$ | flux of species $i$, mol/(cm²-s) |
| $o$ | solvent (water) |
| $P$ | power density, W/cm² |
| $p_i$ | anodic reaction order for species $i$ |
| $P_i$ | pressure of species $i$, atm |
| $q_i$ | cathodic reaction order for species $i$ |
| $R$ | gas constant, 8.314 J/(mol-K) or 82.057 cm³atm/(mol-K) |
| $R_i^e$ | electrochemical reaction rate, mol/(cm³-s) |
| $R_i^b$ | transport rate across phase boundary, mol/(cm³-s) |
| $s_i$ | stoichiometric coefficient of species $i$ |
| $T$ | temperature, K |
| $U_{ref}$ | reference potential, V |
| $u_i$ | mobility of species $i$, mol-cm²/(J-s) |
| $y_i$ | vapor-phase mole fraction of species $i$ |
| $z$ | spatial coordinate, cm |
| $z_i$ | charge number of species $i$ |

### Greek

| | |
|---|---|
| $\alpha^a$ | anodic transfer coefficient |
| $\alpha^c$ | cathodic transfer coefficient |
| $\delta$ | diffusion layer thickness, cm |
| $\epsilon$ | porosity |
| $\eta$ | overpotential, V |
| $\tau$ | tortuosity |
| $\phi$ | solution-phase potential, V |
| $\theta_j$ | parameter $j$ |

### Superscripts and subscripts

| | |
|---|---|
| a | anode |
| c | cathode |
| D | diffusion layer |
| e | electrolyte |
| g | gas phase |
| i | species $i$ |
| j | species $j$ |
| l | liquid phase |
| R | reaction layer |
| r | reference condition |
| S | separator layer |
| + | cation (K⁺) |
| − | anion (OH⁻) |
| * | base-case value |



**Fig. 10. Optimal and base-case power density performance for the alkaline fuel cell.**

## REFERENCES

1. R. P. Iczkowski and M. B. Cutlip, *This Journal*, **127**, 1433 (1980).
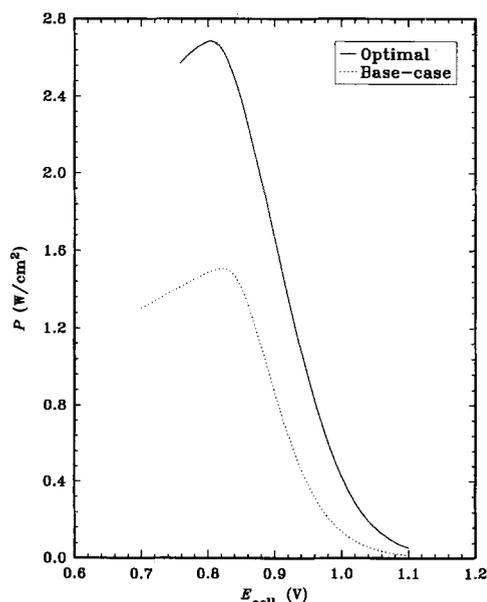2. S. C. Yang, M. B. Cutlip, and P. Stonehart, *Electrochim.*

Acta, **35**, 869 (1990).
3. M. C. Kimble and R. E. White, *This Journal*, **138**, 3370 (1991).
4. T. I. Evans and R. E. White, *ibid.*, **136**, 2798 (1989).
5. T. Kenjo and K. Kawatsu, *Electrochim. Acta*, **30**, 229 (1985).
6. P. Bjornbom, *ibid.*, **32**, 115 (1987).
7. K. E. Gubbins and R. D. Walker, *This Journal*, **112**, 469 (1965).

8. R. E. Davis, G. L. Horvath, and C. W. Tobias, *Electrochim. Acta.*, **12**, 287 (1967).
9. M. K. Tham, R. D. Walker, and K. E. Gubbins, *J. Phys. Chem.*, **74**, 1747 (1970).
10. J. Newman, *Electrochim. Acta*, **24**, 223 (1979).
11. Subroutine BCONF of IMSL library, "Problem-Solving Software System for Mathematical and Statistical FORTRAN Programming," IMSL, Houston, TX (1987).

# Thermodynamic Analysis of Electrochemical Cells Based on a Balance Matrix Theory

## Markku J. Lampinen and Jari Vuorisalo

*Department of Energy Engineering, Helsinki University of Technology, Otakaari 4, SF-02150 Espoo, Finland*

## ABSTRACT

The aim of our research has been to investigate the equilibrium state of electrochemical systems: half cells, fuel cells, and secondary and primary batteries. The analysis presented here is based on the use of a balance matrix theory. The same type of idea has already been used in computer programs for chemical systems, but here it is extended to electrochemical systems. A discharge equation is introduced, with the aid of which the electrochemical cells can be studied at various degrees of discharge. A simple model for electrostatic energy is presented, which enables us also to calculate the charges of the electrodes in the equilibrium state. The advantage of the approach presented here and the motivation for the analysis is that it is easily applicable to computational purposes, even to complicated systems with many phases and also with irreversible constraints. A brief summary of a computer program based on this theory is presented, and the use of the program is illustrated by some examples.

The older methods for equilibrium computation made use of equilibrium constants and the Nernst equation for the cell voltage. As soon as several species appear in the system, the calculation of equilibrium compositions becomes quite complicated, and the complexity is strongly dependent on the number of condensed phases present. In electrochemical systems some of the phases are charged, which makes the problem different compared to chemical systems. In this paper the method of the total free energy minimization, first described by White *et al.* (1) for gas-phase equilibria, is extended to electrochemical systems containing several charged phases. The present method, which is applicable to all equilibrium problems of electrochemical cells, makes no distinction among the constituent species, *e.g.*, the electrons transferred to and from the electrodes are treated like any other constituents of the system. The approach constitutes, for example, a useful computational aid to study the discharge behavior and the stability of batteries.

The electrochemical cell, a thermodynamic system, consists of the electrodes, the gas phases, and the electrolyte surrounding the electrodes. The electrolyte may be in the liquid or solid state. There may also be solid phases in the electrolyte, *e.g.*, some solidified salts. The thermodynamic state of the system can be expressed by the vector $(T, p, n_1, \ldots, n_q)$, where $T$ is the temperature of the system, $p$ its pressure, and $q$ is the number of different species. The molar amounts of different species in the system are denoted by $n_j, j = 1, \ldots, q$ (*e.g.*, $n_1 = n[H^+(aq)]$, $n_2 = n[H_2O(l)]$, $n_3 = n[H_2O(g)]$, ... etc.).

When transformations (chemical and electrochemical reactions, phase transformations) occur in the system, the consequence is that the amounts of species $n_j$ change. The changes in the amounts of the species are constrained by atom balances, by charge balance, and possibly by some additional constraints, which can all conveniently be expressed mathematically by means of the balance matrix $\mathbf{A} = [a_{ij}]$

$$\sum_{j=1}^{q} a_{ij} n_j = b_i \quad i = 1, \ldots s \qquad [1]$$

where $b_i$s are the element, charge, and possibly other amounts which are constants for the closed system (*e.g.*,

$1 \cdot n[H^+(aq)] + 2 \cdot n[H_2O(l)] + 2 \cdot n[H_2O(g)] + \ldots = b[H]$, the amount of hydrogen element in the closed system). $s$ is the number of balance quantities. In addition to the element and charge balances, an important constraint for a total electrochemical cell is Faraday's law, which can also be expressed by Eq. [1] as we shall show below. Some irreversible processes can also be expressed by additional constraints in the form of Eq. [1], as we shall demonstrate by an example in this paper.

When the electric circuit of the electrochemical cell is open, the only outwardly directed work is the expansion work, and then, at constant pressure and temperature, the minimum value of the total Gibbs energy gives the stable equilibrium state of the system

$$G(T, p, n_1, \ldots, n_q) = \text{min!} \qquad [2]$$

The mathematical problem of determining the stable equilibrium state of the system is to find the molar amounts $(n_1, \ldots, n_q)$ which satisfy the constraints [1] and give the minimum value for the total Gibbs energy $G$, *i.e.*, it is a solution of Eq. [2]. The list of species $(j = 1, \ldots, q)$ to be considered must be chosen in advance, and the equilibrium composition is then found for this set of species by using Eq. [1] and [2].

The purpose of this work is to solve Eq. [2] with Eq. [1] for electrochemical systems and to study the consequences. First, the balance matrices are developed for half cells and then for total cells with two or more electrodes. After this, the minimization problem [2] is solved, the cell potential is defined, and some illustrations of the use of the theory are presented.

The objectives of this paper are as follows:

1. To describe the basics of the thermodynamics of electrochemical cells with the aid of a balance matrix. The approach given here differs from the conventional treatment in that we nowhere use reaction equations; the information included in chemical and electrochemical reactions is given here in the form of a balance matrix. For chemical systems this approach is already widely used and accepted [see, *e.g.*, White *et al.* (1), Eriksson (2-4), Smith and Missen (5)]. Here we extend it to electrochemical systems. The important concept introduced here is a discharge equation, which is basically the same as the classical Faraday's law,